Microtremor Measurements in the City of Palermo, Italy: Analysis of the Correlation with Local Geology and Damage

Fabrizio Cara,[1] Giovanna Cultrera,[1] Riccardo Mario Azzara,[2] Valerio De Rubeis[1],Giuseppe Di Giulio,[1] Maria Stella Giammarinaro,[3] Patrizia Tosi[1], Paola Vallone,[3] and Antonio Rovelli[1]

[1] *Istituto Nazionale di Geofisica e Vulcanologia, Via di Vigna Murata, 605, 00143 Rome, Italy*

[2] *Istituto Nazionale di Geofisica e Vulcanologia, Osservatorio Sismologico Centralizzato Aretino, Via Uguccione della Faggiuola,3,I- 52100 Arezzo, Italy*

[3] *Dipartimento di Geologia e Geodesia, Università di Palermo, Via Archirafi, 26, 90123 Palermo, Italy*

To be submitted to BSSA

(October 2007)

Abstract

This study presents the results of 90 seismic ambient noise measurements in Palermo, the main city of Sicily (Italy). The dataset has been processed using the horizontal-to-vertical spectral ratio (HVNSR) technique and interpreted in terms of local geology, which is characterized by the presence of alluvial sediments of two river-beds masked by urbanization since the 17th century. HVNSRs show significant variations in the study area: when the transition stiff-to-soft is crossed, a typical spectral peak appears in the HVNSRs, mostly in the frequency band 1 to 2 Hz, and exceeding a factor of 3 in amplitude. Using available information on sub-surface geological structure we compute theoretical 1- and 2-D transfer functions. The resonance frequencies of soft soils obtained by HVNSR are well reproduced by the fundamental frequencies from numerical modeling.

The distribution of frequency peaks of HVNSR and their amplitudes are also compared with the local damage caused by historical earthquakes. Previous studies demonstrated that damage variations in Palermo were controlled more by near-surface geology than building vulnerability. A uniform vulnerability is an ideal condition to test statistical methods and their capability in seeking correlation between HVNSR and potential damage due to local geological conditions. We apply two well-established multivariate statistical methodologies (factor analysis and canonical correlation) to the HVNSR dataset and macroseismic data (damage grades of the European Macroseismic Scale). Through these analyses we quantify the significance of the correlation between the HVNSR peak in the low-medium frequency range (0.5-3 Hz) and the occurrence of the highest damage grades. This approach allows us *i)* to estimate the threshold value in the resulting linear combination of the HVNSR amplitudes which separates zones of light damage from zones of significant damage, and therefore *ii)* to improve the spatial definition of potentially high hazard zones through a denser grid of microtremor measurements.

Introduction

The damage pattern in urban areas during an earthquake depends on the characteristics of the event and on the interaction between site response and vulnerability of the exposed structures. For seismic hazard assessment, the site effect is typically represented by the resonance frequency and the associated amplification of ground motion. Among several methods (e.g. site-to-reference spectral ratios, horizontal-to-vertical spectral ratios, array data analysis), many authors use ambient noise vibrations (microtremors, hereinafter) to retrieve these parameters. In particular, following Nakamura (1989), the horizontal-to-vertical spectral ratio of microtremors (HVNSR) has been widely used to determine the resonance frequency of a site, and has been applied successfully in urban environments (Duval et al., 2001; Lebrun et al., 2001, Panou et al., 2005). There are many reasons why use of this technique spread very rapidly: (i) it can be applied in regions with low seismicity rate; (ii) a short time of acquisition is required in the field; (iii) low computational time and minimal computing resources are needed to analyze data. The seismological community is still debating about several aspects of the method, both practical and theoretical (Fäh et al., 2001, Malischewky and Scherbaum, 2004, Bonnefoy-Claudet et al., 2006). Open questions are: a) What does

the noise wave-field consist of? b) Is the method really effective in every geological condition? c) Are there standards for operating in the field and for computing HVNSR?

Indeed, successful and unsuccessful experiences have alternated (e.g. Seo, 1998; Bard, 1999; Mucciarelli and Gallipoli, 2001). New advances and overall guidelines have been given by the project SESAME (Site EffectS assessment using AMbient Excitations) funded by the European Commission (SESAME Project, 2001). A significant indication that came out from the project is that the HVNSR method is successful when sites have simple geological structures with strong impedance contrast; in such cases the resonance frequency obtained with microtremors tends to be coincident with that obtained using weak motion recordings although the level of amplification is often underestimated (WP04 of SESAME Project, Deliverable D16.04, 2004; see also Satoh et al., 2001). It was also underlined that the absence of resonance frequencies in HVNSRs does not imply itself the absence of site effects during an earthquake. For this reason, the HVNSR approach should not be used stand-alone for seismic microzonation purposes.

Part of the SESAME project was dedicated to investigating correlation between the HVNSR results and the observed damage distribution during earthquakes. Some studies (e.g.: Lachet et al., 1996; Teves-Costa et al., 2001) find that the HVNSR results are correlated with the spatial distribution of damage when damage variation is controlled by the near-surface geology. In this paper we present results of an experiment performed in the city of Palermo, southern Italy (see the inlet in Figure 1) within the framework of the project. The urban area of Palermo is characterized by high spatial variability of geology, partially masked by urban growth. HVNSRs from 90 noise measurements are first compared to the known geology. Secondly, standard multivariate statistical analyses (Davis, 2002) are used to correlate the HVNSR results with the damage pattern in historical earthquakes, under the assumption that there was limited variation in the vulnerability of buildings beforehand. The availability of geological and damage data allows us to test how the HVNSR technique can be used to get information on site response and statistically quantify its correlation with damage.

Geological Setting and Felt Seismicity

The city of Palermo (Figure 1) was founded on a tectonic depression mostly filled by deposits that are Pleistocene in age. The bedrock of the area is composed of clay and sandstone levels of Oligocene-Miocene age (Numidian Flysch) with local quartzarenite layers. It is unconformably overlain by Plio-Pleistocene sediments (silty-clayey sands and calcarenites). These latter are locally overlain by Holocene sediments that consist of both sea (silts, sands, gravels and calcirudites) and land deposits (sandy silts with peat layers and organic materials, thin sands and clayey silts).

The substratum is incised by the bed of four rivers flowing from south-west to north-east. Two of them, Papireto and Kemonia, were buried and partially filled during the 17th century. They are documented by historical maps and joined in downtown Palermo, flowing into the old harbour (Figure 1). The high level of urbanization now masks their presence. The width of the infill is typically about 150 m, and the thickness of soft deposits increases towards the confluence of the two rivers, from 10 to more than 20 meters for Papireto,

and from 15 to more than 30 meters for Kemonia. A third stream, namely Passo di Rigano, in the northern part of Palermo, is also buried nowadays. The S-SE side of Palermo, adjacent to the historical center, has been influenced by the presence of the Oreto river (Figure 1), which had its path rectified last century. Because of the proximity to its outlet to the sea, the river had a meandering flow and the position of a 12th century (Norman) bridge indicates the different river flow until the 20th century (Figure 1). Alluvial sediments 30-40 m thick are found in this area. Moreover, it is important to mention the presence of remarkable thicknesses of anthropic fillings in large sectors of the city, due to ruins from wars and building debris, and due to human activities, such as quarries.

A high density stratigraphic-geotechnical database has been collected for the area of Palermo (Giammarinaro et al, 2001; Contino et al., 2006). This database contains data of 3000 boreholes with maximum depth up to 180 m. It was the result of a process that required three main steps: *i)* identification and classification of the different lithotypes, *ii)* georeferencing the available boreholes and storing all the information in a Geographic Information System (CITY-GIS) designed to assess natural hazards in urban areas through specific capabilities and queries and *iii)* final data consistency control, exploiting the advantages of the GIS technology.

This GIS allows to reconstruct the geological structure beneath Palermo with high spatial resolution, even though the city is locally characterized by a quickly variable local geology. The presence of several zones interested by thick poorly consolidated sediments, overlying stiffer materials, causes significant amplification of ground motion during earthquakes as documented by Guidoboni et al. (2003) and Di Giulio et al. (2005). The boundaries of the amplification prone zones have been well constrained in downtown Palermo where we have a high density of stratigraphic data, more than 700 boreholes in a area of 2.4 km^2 (Figure 1). In these zones, we distinguish three different geological conditions depending on whether the boreholes find (Al) alluvial deposits, (Sd) recent sea deposits, and (As) alluvial deposits overlain by recent sea deposits (Figure 1).

Although the detailed information on near-surface geology, *in situ* measurements of shear-wave velocities (Vs) are limited in number for each soil type. Other estimates came from laboratory tests, mostly edometric compression (Giammarinaro et al., 2003). The consistency between measured Vs and indirect estimates through laboratory tests is sometimes not strict. Di Giulio et al. (2005) inferred a range of Vs and Q values for the soils through a comparison between experimental transfer functions from small earthquake recordings and 1D-simulations.

The city of Palermo is exposed to moderate seismicity. The Catalog of Strong Italian Earthquakes (Boschi et al., 2000) lists 14 events in the last three centuries that caused Mercalli-Cancani -Sieberg (MCS) Intensity $I \geq V$. Documented damage information in Palermo is available from 1726, when the city was struck by a strong earthquake (September 1, 1726, Imax= VIII-IX MCS). At that time, the urban imprint of Palermo was the same as delineated under the Spanish domination of the city, from the early 17^{th} century up to the first decade of 18^{th} century. The important role of Palermo as capital of the vice-reign of Sicily, led the Spanish to

reinforce the ancient walls, build up new streets and squares and design a new morphology of the area crossed by the Papireto and Kemonia streams. The urban plan was drastically simplified, with the division in four main areas, called “mandamenti”. There the plan of the city was almost the same as we can recognize nowadays. From numerous buildings still standing from that period, we know that the Spanish built one-two storey masonry edifices.

Guidoboni et al. (2003) examined the 1726 earthquake and another two historical earthquakes (March 5, 1823, Imax=VIII MCS; January 15, 1940, Imax= VII MCS) that hit the city causing serious damage. Their analysis of spatial damage variations and near-surface geology showed that the maximum level of damage was well correlated with the presence of the two buried river-beds. While for the 1726 earthquake the vulnerability was uniform, for the other two earthquakes the influence of building vulnerability on observed damage is not so well defined. After the 1726 event, many buildings were poorly repaired and inadequately maintained up until the earthquake in 1823. Moreover, numerous buildings were elevated in subsequent stages up to three to four storeys. The 1940 event occurred in war time, and the macroseismic survey was carried out after the end of the war. Therefore, the seismic damage was disguised by the damage caused by the January-July 1943 bombardments.

On September 6, 2002, an Mw 5.9 earthquake (40 km offshore) caused damage of European Macroseismic Scale (EMS-98, see Grünthal, 1998) Intensity V-VI in downtown Palermo and in its southern sector, the Oreto River valley (Azzaro et al., 2004). Apart from some churches and historical building in the city centre, few structures were seriously damaged. Greater damage occurred in the Oreto River valley, and even there it was sporadic (Giammarinaro et al., 2005). Aftershocks of the 2002, Mw 5.9 earthquake were recorded by eight temporary stations deployed in the urban area on different geological formations (Di Giulio et al., 2005; Calderoni et al., 2005). The locations of some of these stations are shown in Figure 1.

Microtremor survey

Noise measurements were performed at 90 sites in the urban area of Palermo (Cultrera et al., 2004) during 5 days of May 2003. We used six seismological stations equipped with Lennartz Marslite digital recorders and Lennartz Le3D-5sec triaxial velocity sensors. To ensure reliable experimental conditions we followed the guidelines proposed by Koller et al. (2004) in the framework of SESAME (WP02 of SESAME Project, Deliverables D01.02, 2002; D08.02, 2003; and D23.12, 2004). The minimum recording time was 30 minutes. A longer time window was used whenever clear non-stationary sources of noise (cars, pedestrians, markets) occurred. We tried to avoid roads with heavy traffic and underground structures. However, it is important to stress the difficulty in measuring microtremor under controlled experimental conditions in urban environments.

Figures 1 and 3 show the position of measurement sites. In downtown Palermo we recorded along four N/NW-S/SE profiles (D-D’, A-A’, B-B’ and E-E’) crossing the Kemonia and Papireto river-beds, with spatial sampling from 25 to 100 meters between measurement points. The higher sampling there of noise measurements was chosen to increase the resolution across the sharp geological transitions at the edges of

the river-beds. Measurements were performed in a grid configuration in the confluence area, expected to show the largest spatial geology variations. In addition, twelve microtremor measurements were made along a profile crossing the Oreto River valley (C-C'). The CITY-GIS provided by Giammarinaro et al. (2001) allowed us to quickly locate the measurement points taking into account buildings, streets and borehole information.

Microtremor data were analyzed using software implemented within the SESAME consortium (WP03 of SESAME Project, Deliverable D09.03, 2003). We selected the stationary portion of the whole signal using at least 10 windows of 25-60 sec length. Each window of signal was detrended and 5% cosine tapered, FFT transformed and then smoothed using the Konno and Omachi (1998) algorithm with a b value of 40. We tried several procedures of smoothing, without significant differences in the results. No filtering before FFT was applied. A check was made to guarantee the absence of anthropic disturbances, i.e. monochromatic sources (see Figure 2). The two horizontal components spectra were combined into root-mean-square values before dividing by the vertical component spectrum. Finally, the geometric means and standard deviations of the HVNSRs were calculated for frequencies greater than 0.4 Hz, which was chosen to avoid the eigenfrequency of the sensor (0.2 Hz).

Following the SESAME recommendations (WP02 of SESAME Project, Deliverables D23.12, 2004), we visually selected frequency peaks with amplitude greater than 2. This threshold value was adequate in Palermo, since we found that flat HVNSRs had no clear frequency peaks with amplitude below 2. Further details of the criteria for the selection of the peaks are discussed by Cultrera et al. (2004).

Spectral Analysis - Correlation Between HVNSRs and Geology

Results show large variability in the shape of HVNSRs. Based on the frequency of the HVNSR peak and its amplitude, the measurement sites were classified into 2 classes of frequencies (1.4-1.9 Hz, and 2.0-2.8 Hz) and 3 classes of amplitudes (2-3, 3-4.5, and 4.5-6).

Figures 3 and 4 show the comparison between HVNSR results and geological setting in downtown Palermo. Geological cross-sections in Figure 4 were reconstructed using at least one well log every 90 meters, not farther than 10 m from the profile for the Papireto River, and 30-40 m for the Kemonia River. Note that these distances are to be compared with the order 100-150 m widths of the river valleys.

The spatial distribution of the classes involves: i) occurrence of frequency peaks in the areas of the Kemonia and Papireto rivers; ii) absence of clear peaks, or presence of peaks with HVNSR amplitude below 2, at sites without soft soils at the surface. Peak frequencies within the Kemonia and Papireto river-beds (profiles A-A' and D-D') are in class 2 (see Figure 4 where details of each profile are displayed). From profile D-D' in the west to profile E-E' in the east, the sediments deepen and the frequency peak values decrease to class 1: we found the lowest values of frequency in the confluence zone (profiles B-B' and E-E'). A possible explanation is the major thickness of soft soils due to sea and alluvial deposits, but lower wave velocity of the soils may contribute as well.

Moving from the middle to the edges of the river-beds we did not find any increase in the resonance frequency. Even where we increased the number of sites to improve the resolution in these zones, the spatial sampling we used was not adequate to map the transition from frequency class 1 to frequency class 2.

The distribution of amplitudes of the HVNSR peaks confirms the relationship with the presence of soft sediments: in this case, the threshold of 2 appears to be appropriate to distinguish stiff and soft sediments. Highest values (amplitude class 3) are limited to few small areas of the confluence zone and close to the harbour (profiles B-B' and E-E', respectively). Overall, the distribution of HVNSR amplitudes within the three classes is very irregular with amplitudes in different classes at closely spaced sites. Beyond the fixed threshold, amplitude of HVNSR peaks is an indicator of the occurrence of a resonance frequency peak but at the moment no theoretical basis exists to attribute a physical meaning to variations of amplitude (see previous studies: Lachet et al., 1996; Satoh et al., 2001). It is worth noting that Di Giulio et al. (2005) found lower amplifications from HVNSR, at the resonance frequencies, than from analysis of earthquakes. For example, station PAL5, along the profile B-B' (see Figure 1), has a resonance frequency from HVNSR that, consistently with close measurements, is in frequency class 1. In the earthquake analysis using classical site-to-reference spectral ratios, the amplification of ground motion at PAL5 reaches values up to 10 in the same frequency class.

According to the criterion of Bard and Bouchon (1985), the Vs values proposed by Di Giulio et al. (2005) and the widths of the two river valleys indicate that 2D resonance is possible in areas where the sediment thickness is larger than 20m. To investigate whether the HVNSRs are representative of the S-wave earthquake amplification, we performed 2D simulations along the A-A' profile and we compared the results with those of the HVNSR analysis (Figure 5). We used a finite-difference code (Caserta et al., 2002) which computes displacement time series at the free surface using a vertically incident delta-like (Gabor) function as SH plane-wave input in the frequency band of 0-7 Hz. To obtain the 2D theoretical transfer functions, we smoothed the amplitude Fourier spectrum of each synthetic seismogram with a 0.5 Hz window and divided it by the corresponding reference spectrum for a half-space model. The geological setting and geometry of profile A-A' are shown in Figure 5a. In order to fit the resonance frequencies of HVNSR in the middle of the valleys we had to increase the Vs of alluvial sediments used by Di Giulio et al. (2005) by 25% (from 200 m/s to 250 m/s, see table 1). Note that this increment in Vs is compatible with the uncertainty in the resonance frequency depicted through HVNSR (Bonnefoy-Claudet et al., 2006). Using this velocity model, the comparison of 2D transfer functions with HVNSR contour maps is shown in Figures 5b and 5c, as a function of frequency and position along the profile. The fundamental resonance frequencies of the 2D simulation reproduce fairly well the HVNSR peaks of the sites in the middle of the river-beds. Note the higher spectral complexity in the 2D simulation compared to the HVNSR results. Figure 5d shows the comparison of the amplification curves (2D and HVNSR) at sites A6, A3 and A16. For station A6, in the middle of the Papireto river valley, the fundamental frequency from HVNSR agrees with that estimated using 2D modeling. Stations A3 and A16 are very close to seismic stations PAL2 and PAL6, respectively, for which horizontal-

to-vertical spectral ratios from earthquakes are available (see Figure 1). At the edges of the river-beds (sites A3 and A16), the resonance frequencies from the 2D simulation differ from those obtained by HVNSR. Earthquake transfer function for PAL6 is more similar to HVNSR than the 2D result. In contrast, station PAL2 shows earthquake amplification at high frequencies whereas the HVNSR is almost flat (see Figure 5d). This result suggests that amplification of earthquake ground shaking is possible also at sites with flat HVNSR (Koller et al., 2004, WP02 of SESAME Project, Deliverables D23.12, 2004).

Taking into account all these limitations, the uncertainties of profile reconstruction in such a complicated geological framework could lead to bias in the modeling results, such as the shift in the zone of maximum amplitude observed along profile A-A' (Figures 5b and 5c). 1D transfer functions (not shown in the figure) indicate slight differences from the 2D simulation. However, our results suggest that (*i*) within the river-beds, the HVNSR technique is able to detect the fundamental resonance frequencies predicted by 1D and 2D modeling, whereas it does not show the higher modes of the theoretical transfer functions (see Bard, 1999); (*ii*) at sites close to the edges of the river-beds, the differences between HVNSR, spectral ratios in earthquakes and numerical transfer functions indicate that the complexity in site response due to the complicated geology cannot be fully represented by 1D or 2D numerical simulations.

During the September 6, 2002 earthquake, buildings in the Oreto River valley (see Figure 1) suffered scattered instances of damage (Giammarinaro et al., 2005). Significant amplifications in this area (see Figure 1, station PAL9) were found by Di Giulio et al. (2005). We performed noise measurements along a profile crossing the river (C-C' in Figure 1). The top panel of Figure 6 shows the distribution of boreholes around the measurement profile. These were too sparse for reconstruction of the geology to adequately represent the complexity of this region (Figure 1 and Figure 6, bottom). Indeed, the number of logs is high only in restricted areas close to sites #42, #45, #46, #47 and #48. A further issue is the rectification of the Oreto river during the 20th century. Topographic variations and the presence of ruins of a Norman bridge (12th century) reveal that the original flow of the river was meandering and indicate that its previous path was southward of the present one.

The results of the HVNSR analysis for profile C-C' are shown in Figure 6. Sites from #39 to #44 show similar broad peaks around 1-1.2 Hz with low amplitude values of 2-3, even though they have different geological conditions: the first three sites (#39 to #41) are in an area with 5-8 m thick layers of sea deposits overlaying calcarenites and silty sands, whereas the others (#42 to #44) are in the alluvial deposits of the river. Narrow frequency peaks around 1.2-1.8 Hz with large amplitude values (up to 6) occur on the right-hand side of the current river, from sites #45 to #48 (see HVNSR of site #45 in Figure 6). These peaks are related to low S-wave velocity associated either with alluvium infilling of the river valley or the presence of a quarry filled in historical times with soft materials.

In view of the lack of detailed geological information along the profile, we computed only the 1D transfer functions of vertically-incident SH waves (Thomson, 1950; Haskell, 1953) at specific sites using nearby borehole data. The correlation between HVNSR peaks and thickness and S-wave velocity of the underlying

materials (Table 1) was investigated in particular at site #45, which is representative also of #46 and #47. Results there show that HVNSR peaks are in good agreement with the fundamental frequency of the 1D transfer function (Figure 6).

Finally, the last two sites (#49 and #50) have broad HVNSR peaks around 1-2 Hz with amplitudes of 3 but with very large standard deviations (see HVNSR of site #49 in Figure 6).

The joint analysis of frequency peaks and amplification of HVNSRs with subsurface geology outlines the capability of the HVNSR method to reveal the presence of soft sediments in Palermo, especially when there is a strong impedance contrast at the underlying bedrock. This conclusion is particularly important because it is very difficult to achieve the same results in urban areas using other low-cost geophysical techniques. The geological configuration of the Kemonia, Papireto and Oreto valleys permits the mapping of fundamental frequencies of sites using the HVNSR method and from that the estimation of sediments thickness. Less reliable results are found in zones where the spatial variability of sediments is high, such as at the edges of river-beds and the transition zones between fluvial and sea deposits. Moreover, the comparison of HVNSR from microtremors with SH-wave simulation of 1D or 2D models shows that HVNSR fails in reproducing the higher modes of the simulated transfer functions. This is commonly observed at soft sites (e.g., see Cara et al., 2003). The amplitude of HVNSR peaks in Palermo underestimates the S-wave amplification both from synthetics and earthquake data, as also observed by Di Giulio et al. (2005). Therefore, the amplitude information can improve knowledge of local geological conditions but can not be used as a direct estimate of site amplification.

Statistical Analyses - Correlation Between HVNSRs and Damage

A further aim of this study is to verify whether the damage pattern in strong earthquakes can be associated with the HVNSR variations. Due to the scattered nature of the damage in the Oreto River valley during the 2002 earthquake (Giammarinaro et al., 2005) and the absence of information there for past earthquakes, we restrict this analysis to the downtown Palermo area.

As already mentioned, the highest levels of earthquake damage in downtown Palermo are due to the presence of sea and alluvial sediments, and these have been identified using HVNSRs in the present study. In this section we use statistical methods to assess whether and to what extent the occurrence of damage in the city of Palermo is related to the frequency distribution of HVNSR peaks and/or their amplitudes.

In Figure 7 we overlay the results of the HVNSR analysis and the damage distribution of the strongest event analyzed by Guidoboni et al. (2003), i.e. the September 1, 1726, earthquake (Imax= VIII-IX MCS). We have translated the damage description of these authors to damage grades of the EMS according to the Grünthal (1998) prescriptions. This operation was possible because the type of construction was quite homogenous at the time of the earthquake, with the vulnerability of the buildings being moderate to high but without strong spatial variations (Table 2).

The presence of a resonance peak in the HVNSRs coincides well with the occurrence of damage and the largest amplitudes of HVNSR peaks are observed close to the zones where the highest grade of damage occured (Figure 7). However, the change of the frequency class does not always result in a change of the damage class. This is probably due to the range of the two frequency classes (1.4 to 2.8 Hz) which includes the building resonances of the types of structure in downtown Palermo (3 to 5 stories).

To quantify the extent of the correlation, for each class of damage in the 1726 earthquake we calculated the histograms showing the number of sites where the different frequency peaks and amplitudes are found (Figure 8). For comparison we also show corresponding results for the cumulative effect of the 1726, 1823 and 1940 earthquakes studied by Guidoboni et al. (2003). Some features emerge from this analysis:

i) Most of the HVNSR measurements show insignificant amplification (< 2: also denoted as frequency <1) where damage grades 0 to 2 are observed; this is more evident when considering the cumulative damage of the three earthquakes studied by Guidoboni et al. (2003) (Figure 8b). However, a frequency peak with amplitude over 6 and a few up to 5 appear for the 1726 earthquake (Figure 8a) in the same range of damage grades.

ii) For the damage class 3, several frequency peaks in the range 1-2 Hz and even more in 2-3 Hz have amplitude of 2 to 4. Of the 28 HVNSR measurements in this class 5 do not show a peaked frequency (amplitude < 2; frequency < 1).

iii) All sites in damage class 4 show a peaked frequency. Most of the observed HVNSR peaks are in the 1-2 Hz class, with amplification of 3-5.

This kind of semi-qualitative analysis does not provide a quantitative relation between HVNSR and damage. To give a more detailed statistical interpretation, we applied two multivariate statistical analyses (factor and canonical correlation analyses).

We considered EMS damage grades and HVNSR of the 78 sites in downtown Palermo as elements of a multivariate data set. For damage we used the values of the 1726 and 1823 earthquakes and the cumulative effect quantified by Guidoboni et al. (2003) as the prevalent maximum level of damage (above 50%) of the three earthquakes 1726, 1823 and 1940, occurring in buildings within each 100 m by 100 m square cell. In our analysis we did not use the damage in 1940 event as a stand-alone variable because of the uncertainties in the macroseismic survey. Similarly, we have not considered damage in the 2002 event because of the generally low level of damage in the downtown area, where macroseismic information is also poor (Giammarinaro et al., 2005). Furthermore, it is important to note that both the damage pattern in the 1823 event and the cumulative effect are significantly driven by the effects of the 1726 earthquake, which was the strongest of the events and before which the buildings had comparatively uniform vulnerability to damage.

For the statistical analyses below, the continuous spectra of HVNSRs from microtremor data have been segmented into nine 0.5-Hz-wide frequency intervals, from 0.5 to 5.0 Hz. In each interval the logarithm of the mean amplitude has been computed. We have checked that these mean-amplitude values for each site have in general a log-normal distribution, which is a requirement for the statistical analyses.

Therefore, each site has 12 variables: nine of them represent the logarithm of the HVNSR mean amplitude in the 0.5 Hz frequency intervals; the other three variables are the damage degree of the two earthquakes and the cumulative damage value of the three events. The whole data set has been organized in a (78 x 12) matrix, $[X_{raw}]$.

The first multivariate approach we used is factor analysis (Davis, 2002). This method is suitable for finding interrelationships among variables. The result of the analysis is a representation of the original data set as linear combination of uncorrelated new variables, called factors. The elements of the factors a_{ij} are referred to as *factor loadings* and define a (12 x 12) matrix $[A^R]$ in which each column *j* represents a factor and each row refers to an original variable *i*. A description of the factor analysis and the definitions of the associated statistical quantities are given in Appendix A.

Because of the way the factors are calculated, each factor loading is weighted in proportion to the square root of the variance contributed by that variable to the factor. In Figure 9a the proportion of the total variance accounted for by each factor is shown. Note that the first two factors each accounts for more than 30% of the total variance, and almost 70% when summed together (Figure 9b). This result strongly indicates that our data reflect the behavior of only two independent factors (factor 1 and factor 2). Therefore, we can reduce the effective size of $[A^R]$ to 12 x 2.

Figure 10 shows the factor loadings of the original variables for both factors. Factor 1 represents very well a direct correlation of HVNSR log-amplitudes within the 0.5-3.0 Hz frequency range with all the three seismic damage variables. Factor 2 represents the higher frequency intervals (3.0-5.0 Hz) with no correlation with damage. Note that the slightly higher correlation given by the cumulative damage in Factor 1 may be due to an effective reduction in noise generated by merging the damage datasets from the three earthquakes.

These results can be summarized as follows: (i) damage grades are stable, meaning that different events have the same behaviour at each site (Figure 10a); (ii) damage grades are directly related to the lower-medium frequency portion (0.5 Hz < f < 3.0 Hz) of log amplitude of HVNSR (Figure 10a); (iii) high frequencies (3.0 Hz < f < 5.0 Hz) also have a coherent behaviour, but there is no relation with damage (Figure 10b). Finally, the two main factors represent the meta-variables that drive our site behavior both for damage and microtremor.

It is also possible to plot the geographic distribution of each factor (factor scores; see Appendix A). In Figure 11 we show the spatial distribution of factor 1: high values of the factor scores represent both high values of damage grades and high values of log-amplitude in the 0.5-3.0 Hz frequency band (Figure 10), and in particular they delineate the zones of fluvial deposits in the west of the study area.

Factor analysis is effective in exhibiting relationships among variables. It does not provide statistical tests of the significance of results, even though an indication is given by the variance accounted for by each factor. Another limitation of factor analysis is that variables are grouped together with no quantification of their relationships.

To further validate results and to fulfil the interpretation gap left by factor analysis, we performed canonical correlation analysis. A description of this analysis and the definitions of the associated statistical

quantities are given in Appendix B. The goal is to relate a set of dependent variables (EMS damage grades) to a set of independent variables (HVNSR mean amplitude in 0.5 Hz wide frequency bands) by finding linear combinations of the variables that give the highest correlations between the two sets.

Let us call $[Y]$ the matrix of damage, composed of 78 observations of 3 variables, and $[X]$ the matrix of log-amplitudes of 0.5 Hz bands, composed of 78 observations of 9 variables. The aim of this analysis is to find two vectors $[A]$ and $[B]$ of 3 and 9 elements respectively, in a way that the linear transformations

$$[Y_{can}] = [Y] \cdot [A]$$
$$[X_{can}] = [X] \cdot [B]$$

will produce the highest possible correlation between them. Moreover, the variances of the two new sets of variables are constrained to be equal to one, so that the maximized covariances become maximized correlations.

With $[Y]$ composed of observations of 3 variables, the analysis allows to transform the two original variable groups ($[X]$ and $[Y]$) into three couples of canonical variables ($[X_{can}]$ and $[Y_{can}]$: they are 78-elements vectors), and each having a correlation coefficient *r*. The significance of the three canonical correlations is assessed by means of the Rao's scoring test (Rao, 1973). Table 3 shows that, among the three possible canonical correlations, only the highest one (equal to 0.717) is statistically significant, with 0.01% probability of being a correlation without meaning. Figures 12a and 12b show the vectors $[A]$ and $[B]$ for the couple with this best correlation. They represent the weights used to transform the original variables into the best canonical variables. Consistent with the behaviour of factor 1 in factor analysis, low-medium frequencies are directly correlated to damage.

The selected couple of canonical variables for each site *j* are plotted in Figure 13a. They are expressed through the combined damage $Y_{can,j} = \sum_{i=1}^{3} Y_{ji} A_i$, where A_i is the canonical correlation coefficient relative to the original damage variable Y_{ji} at each site *j* (Figure 12a), and the combined HVNSR variables $X_{can,j} = \sum_{k=1}^{9} X_{jk} B_k$, where B_k is the canonical correlation coefficient relative to the original variable X_{jk} also at site *j* (Figure 12b). The distribution of the elements of $[X_{can}]$ and $[Y_{can}]$ is fitted best by the regression line

$$y_{can} = 0.72 x_{can} + 1.62$$

Figure 13b shows that $[Y_{can}]$ follows a bimodal distribution; this behaviour reflects the distribution of the original damage variables (Figure 8), which are mostly concentrated in two classes: no or light damage and significant damage. This leads us to define a threshold value of y_{can} corresponding to the separation of the two modes and equal to 2.7 (Figures 13a and 13b).

This makes it possible to assess whether a site within the studied area of Palermo was likely to have suffered a negligible or important level of damage in the earthquakes considered. From HVNSR of microtremors we can retrieve a value of the canonical variable x_{can} for the given site. The corresponding canonical variable y_{can} is then computed using the regression line above: if the computed y_{can} value is below the defined threshold we can expect negligible damage, whereas beyond it we expect there to have been an important level of damage. Note that by definition y_{can} does not follow the same scale as the original damage variables: we are not able to use it directly to estimate the EMS damage grade but we can estimate relative damage behaviour.

Taking into account the threshold of y_{can}, we can look at the geographical distribution of this canonical variable (Figure 14). This closely confirms the general result from the factor analysis, of damage and HVNSR being strictly related to the presence of fluvial deposits.

Discussion and Conclusions

In the present study we have investigated the use of HVNSR analysis using microtremors in the city of Palermo to map the fundamental frequency of soils, which depends on the ratio between shear wave velocity and thickness of the upper soft layers. We have also sought possible statistical correlations between HVNSRs and the damage experienced during moderate earthquakes.

Palermo represents a typical Italian urban context, with very important historical heritage damaged by several earthquakes both in the past and in recent times. Previous investigations, based on a dense set of macroseismic data, indicated that variations of near-surface geology play an important role in increasing the seismic hazard in the area of downtown Palermo crossed by two buried river-beds (Guidoboni et al., 2003). This study benefits from abundant data on local geology and damage distribution. A very large number of boreholes and geological surveys were respectively collected and conducted by the University of Palermo (Giammarinaro et al., 2001), and these data have been used in this study to retrieve very local information and reconstruct the geological structure beneath the study area.

Ninety microtremor measurements were performed along several profiles crossing the soft sediment bodies. The results indicate that the ambient noise analysis can be an efficient tool for exploring soil conditions in urban areas, under the hypothesis that the velocity contrast between soft sediments and the bedrock is large. In particular, we have assessed the link of HVNSR with soft soil characteristics (thickness and shear wave velocity), comparing the HVNSR resonance frequencies with the results of 1-and 2-D numerical models. Although the amplitude of HVNSR in itself is not a measure of local transfer function amplitude, the pattern of peaked frequencies and amplitudes of HVNSR are successful in recognizing the zones in Palermo where sediment amplification occurs.

Moreover, we have investigated the correlation between HVNSR and the damage distribution from past earthquakes. This comparison is generally biased by several factors that affect the damage pattern, such as

the influence of the earthquake source, the weakness of the existing buildings, and vulnerability changes following a previous earthquake. However, in the case of downtown Palermo, Guidoboni et al. (2003) showed that the damage distribution is mostly controlled by the presence of soft deposits, given that the vulnerability originally was essentially uniform over a large area. We then applied two statistical tools (factor analysis and canonical correlation) to retrieve a quantitative correlation of the resonance frequency and the amplitude of HVNSRs with the record of damage. The factor analysis leads to a simplification of the problem, combining the original variables into only two factors that in our case appear to be significant. One is the logarithm of HVNSR mean amplitude in the low-medium frequency range (0.5-3 Hz) that is directly correlated with the level of damage, the second one is the logarithm of HVNSR mean amplitude in the high frequency range (3-5 Hz) that does not show any correlation with the level of damage. In general, the building resonance frequency (f_r) depends on the number of floors. In Palermo we have mainly 3-5 stories buildings and we expect a f_r of about 2-3 Hz. This is confirmed by Di Giulio et al. (2005) who found similar consistent values of f_r (2-3 Hz) by analyzing simultaneous microtremors at the top and at the bottom of some buildings in downtown Palermo. Therefore, the low-medium frequency range includes the resonance frequency of the predominant building type in Palermo.

After the factor analysis, the canonical correlation analysis gave further insights with a statistical test on the significance of the correlation, by grouping the variables according to their mutual relationships. For our problem this approach constructed a pair of related canonical variables which are a linear combination of the HVNSR mean amplitudes and a linear combination of the EMS damage grades, respectively. Their correlation is statistically significant. The distribution of the damage canonical variable follows a bimodal distribution, like that observed for the original damage values from each earthquake, mostly concentrated into two classes (no-or-light damage and significant damage). The threshold between the two sets of damage values led us to separate the HVNSR canonical variable values into two groups, which correspond to either negligible or important level of damage during the earthquakes considered. In principle, by extending the HVNSR measurements to other sites where we do not have damage information, we can assess the probability that those sites are exposed to significant damage. It has to be underlined that the validity of the proposed statistical methodology is constrained by the damage in the earthquakes used for the analysis and reflects the vulnerability conditions at the times of the earthquakes. Therefore, hazard considerations can be translated into risk only if vulnerability conditions do not change in time. Moreover, the larger the number of the macroseismic datasets, the more reliable the relationships between the canonical variables.

In conclusion, we have established a statistical link of HVNSRs with soft soil characteristics and damage distribution in downtown Palermo. Although there is no theoretical basis to assume that amplitude of HVNSR is related to real amplification, we find a positive correlation between amplitude of the HVNSR peaks and level of damage. A possible explanation could be that sites characterized by the largest amplification during earthquakes also show the highest amplitudes of HVNSR.

Several peculiarities of the case study of Palermo helped in this analysis: *i)* the resonance frequency of soils estimated from HVNSR and the damage distribution are well controlled by site amplifications due to

the presence of soft sediments; *ii)* the vulnerability was substantially uniform in the analyzed area when the strongest earthquake occurred; *iii)* exhaustive macroseismic datasets were collected for more than one earthquake. The quantitative and robust correlations found in this study are limited to downtown Palermo and can not be extrapolated to assess the damage distribution in other areas with different site conditions. However, an approach combining damage reports and microtremor measurements seems to be potentially successful, suggesting interesting low-cost perspectives in the practice of territory planning and zoning in urban areas.

Acknowledgments

This work was performed within the framework of the "SESAME" project, supported by the Environment and Sustainable Development Program of the European Commission Research Directorate General (Contract No: EVG1-CT-2000-00026). We thank the students of Palermo University who helped us during the experiment. Special thanks are due to Professor John Haines of Cambridge University for reading and checking the text and to the two anonymous reviewers of the manuscript. Their constructive comments considerably improved many parts of this article.

Appendix A

Factor analysis (Davis 2002)

The factor analysis is a multivariate approach suitable to find mutual relation among variables. The original data set is defined as the ensemble of *n* observations of *m* variables, arranged in a (*n* x *m*) matrix $[X_{raw}]$. In factor analysis, the common assumption is that all *m* variables of the original data set descend from a smaller set of *p* independent factors ($p < m$).

We followed the principal component approach to factor analysis which consists of the following steps. First, the original raw data $[X_{raw}]$ are standardized by subtracting the means and dividing by the standard deviations related to each variable, obtaining the matrix $[X]$. Second, the standardized variance-covariance (correlation) matrix $[s^2]$ is calculated; it is symmetric and the diagonal elements are equal to 1, that is standardized data $[X]$ have zero means and unit standard deviations. Third, eigenvectors and eigenvalues are extracted from $[s^2]$; the eigenvectors define the matrix $[U]$ and the square roots of eigenvalues define the diagonal matrix of singular values $[\lambda]$; the sum of the eigenvalues represents the total variance (information content) of our data. Fourth, the eigenvectors are converted into factors by using the relation:

$$[A^R] = [U] \cdot [\lambda], \tag{1}$$

where $[A^R]$ is a (*m* x *m*)-sized matrix, each column representing a factor whose elements are referred to as *factor loadings*. Because of the way the factors are calculated, each factor loading is weighted proportionally to the square root of the amount of variance contributed by that variable to the factor. Looking at the proportion of variance accounted for by each factor, it is possible to select a smaller number of factors (*p*) accounting for most of the total variance in the dataset. The independence of all factors is guaranteed by orthogonal decomposition of the correlation matrix, given by the Eckart-Young theorem, through the extraction of eigenvalues and eigenvectors. Therefore, we can reduce the size of $[A^R]$ to *m* x *p*.

Factor analysis results in factor scores $[\hat{S}^R]$, which represent the values of any single factor for every observation, as follows:

$$[\hat{S}^R] = [X] \cdot [A^R] \cdot \left([A^R]^T \cdot [A^R] \right)^{-1} \tag{2}$$

In this way it is possible to associate with each observation the value of a factor score related to each one of the *p* factors. Adding the geographical coordinates, we obtain the distribution over the territory of these factor scores.

Appendix B

Canonical correlation analysis (Davis 2002)

The goal of the canonical correlation analysis is to relate a set of dependent variables $[Y]$ to a set of independent variables $[X]$ by finding linear combinations of the variables that give the highest correlations between the two sets. The matrix $[Y]$ consists of *n* observations of *i* variables, and $[X]$ of *n* observations of *j* variables.

The matrix of variance-covariance of the composition of both groups of variables can be expressed as:

$$[S] = \begin{bmatrix} S_{yy} & S_{xy} \\ S_{xy}^T & S_{xx} \end{bmatrix} \tag{3}$$

where $[S_{xx}]$ is the *j* x *j* matrix containing the variances and covariances of $[X]$, $[S_{yy}]$ is the *i* x *i* matrix containing the variances and covariances of $[Y]$ and $[S_{xy}]$ is a *i* x *j* matrix ($[S_{xy}^T]$ is its transpose) containing the covariances between $[X]$ and $[Y]$. This analysis is aimed at finding two vectors $[A]$ and $[B]$ of i and j elements respectively, in a way that the linear transformations

$$\begin{aligned} [Y_{can}] &= [Y] \cdot [A] \\ [X_{can}] &= [X] \cdot [B] \end{aligned} \tag{4}$$

will produce the highest possible covariance expressed as $[A]^T \cdot [S_{xy}] \cdot [B]$ where $[A]^T$ is the transpose of vector $[A]$. Moreover, the variances of the two new sets of variables are constrained to be equal to one, that is:

$$\begin{aligned} [A]^T \cdot [S_{yy}] \cdot [A] &= 1 \\ [B]^T \cdot [S_{xx}] \cdot [B] &= 1 \end{aligned} \tag{5}$$

where $[B]^T$ is the transpose of vector $[B]$.

In such a way the maximized covariances become maximized correlations. If we solve the equation:

$$|([\Lambda] - \lambda[I])| = [0] \tag{6}$$

where $[\Lambda] = [S_{xx}]^{-1}[S_{xy}]^T [S_{yy}]^{-1}[S_{xy}]$ is (*i* x *i*)-sized, we find *i* eigenvalues λ_i, that are numerically equal to the square of the correlation between the two canonical variables $[X_{can}]$ and $[Y_{can}]$. Substituting them into:

$$([\Lambda] - \lambda[I]) \cdot [B]^T = [0] \tag{7}$$

we obtain the vector $[B]$.

$[A]$ is found as:

$$[A] = \left[[S_{yy}]^{-1} \cdot [S_{xy}] \cdot [B] / \sqrt{\lambda} \right]^T \quad (8)$$

Substituting the three values of λ into relation (7) and (8) and then the resulting $[A]$ and $[B]$ into (5) we transform the two original variable groups into *i* couples of canonical variables ($[X_{can}]$ and $[Y_{can}]$, *n*-elements vectors) having correlation $r = \sqrt{\lambda}$. Note that we have reduced the size of the problem to the minimum number of variables in the two sets of original variables $[X]$ and $[Y]$, equal to *i*.

Moreover, we can investigate the significance of the three canonical correlations by means of specific statistical tools. In particular we use the Rao's scoring test (Rao, 1973), which gives the probability to randomly have a score F (associated to the respective degrees of freedom), that is the probability to have a correlation with no meaning. This test allows to select the best couple of canonical variables whose canonical correlations are statistically significant.

References

Azzaro, R., M. S. Barbano, R. Camassi, S. D'Amico, and A. Mostaccio (2004). The earthquake of 6 September 2002 and the seismic history of Palermo (Northern Sicily, Italy): implications for the seismic hazard assessment of the city, *J. Seism.* **8,** 525–543.

Bard, P.-Y., and M. Bouchon (1985). The two-dimensional resonance of sediment-filled valleys, part II: The case of incident *P* and *SV* waves, *Bull. Seism. Soc. Am.* **75,** no. 2, 519–541.

Bard, P.-Y. (1999). Microtremor measurements: A tool for site effect estimation?, in *The Effects of Surface Geology on Seismic Motion*, Irikura, Kudo, Okada, and Sasatani Eds., 1251-1279, Balkema, Rotterdam, Netherland.

Bonnefoy-Claudet, S., C. Cornou, P.-Y. Bard, F. Cotton, P. Moczo, J. Kristek and D. Fäh (2006). H/V ratio: a tool for site effects evaluation. Results from 1-D noise simulations, *Geophys. J. Int.*, **167**, 827–837.

Bonnefoy-Claudet, S., F. Cotton, P.-Y., Bard, C. Cornou, M. Ohnrberger, M. Wathelet, (2006). Robustness of the H/V ratio peak frequency to estimate 1D resonance frequency, *Third International Symposium on the Effects of Surface Geology on Seismic Motion, France, 30 August - 1 September 2006,* Paper # 85.

Boschi, E., E. Guidoboni, G. Ferrari, D. Mariotti, G. Valensise and P. Gasperini (Editors) (2000). Catalogue of strong Italian earthquakes from 461 B.C. to 1997, version 3 of the Catalogo dei Forti Terremoti in Italia, *Ann. Geofis.,* **43**, no. 4, 609-868.

Calderoni, G., A. Rovelli, G. Cultrera, R.M. Azzara, and G. Di Giulio (2005). Assessment of round motions in Palermo (Italy) during the September 6, 2002 Mw 5.9 earthquake, *Bull. Seism. Soc. Am.* **95,** no. 6, 2342–2363.

Cara, F., G. Di Giulio, and A. Rovelli, (2003). A study on seismic noise variations at Colfiorito, central Italy: implications for the use of H/V spectral ratios, *Geophys. Res. Lett.*, **30**, no. 18, 1972, doi:10.1029/2003GL017807.

Caserta, A., V. Ruggiero and P. Lanucara (2002). Numerical Modelling of dynamical interaction between seismic radiation and near-surface geological structures: a parallel approach, *Computer & Geosciences*, **28**/9, 1071-1079.

Contino A., M.S. Giammarinaro, P. Vallone, S. Varsalona, A. Zuccarello (2006). Analisi stratigrafico –

geotecnica del settore meridionale della città di Palermo finalizzata alla caratterizzazione di fattori di pericolosità sismica in esso presenti. *Boll. Soc. Geol. It.*, **125**, 329-343.

Cultrera G., R. Azzara, F. Cara, R. d'Anna, G. Di Giulio, M. S. Giammarinaro, G. Passafiume, A. Rovelli and P. Vallone (2004). Microtremor Measurements in Palermo, Italy: a comparison with macroseismic intensity and earthquake ground motion. *Proceedings of the 13th World Conference on Earthquake Engineering, Vancouver, August 2004,* Paper # 915.

Davis, J.C. (2002). Statistics and Data Analysis in Geology, third edition, *Wiley and Sons, Inc.*, New York.

Di Giulio, G., R. M. Azzara, G. Cultrera, M. S. Giammarinaro, P. Vallone, and A. Rovelli (2005), Effect of local geology on ground motion in the city of Palermo, Italy, as inferred from aftershocks of the September 6, 2002, M_w 5.9, *Bull. Seism. Soc. Am.*, **95**, no. 6, 2328-2341.

Duval, A.M., S. Vidal, J.-P. Méneroud, A. Singer, F. De Santis, C. Ramos, G. Romero, R. Rodriguez, A. Pernia, N. Reyes and C. Griman (2001). Caracas, Venezuela, Site effect determination with microtremors, *Pure appl. Geophys*., **158**, 2513-2523.

Fäh, D., F. Kind, and D. Giardini (2001). A theoretical investigation of average H/V ratios, *Geophys. J. Int.* **145**, 535-549.

Giammarinaro, M. S., E. Guidoboni, S. Maiorana, D. Mariotti and A. Rovelli (2001). A Gis System as a tool for the integrated analysis of geological data and seismic effect: Historical Centre of Palermo. *IEEE/ ISPRS Joint Workshop on Remote Sensing and Data Fusion over Urban Areas*. 288-292.

Giammarinaro, M.S., V. Canzoneri, P. Vallone, and A. Zuccarello (2003). Effects of the September 6th, 2002 earthquake: damage amplification in the south-eastern sector of Palermo explained through GIS technology, *Annals of Geophysics,* **46** (6), 1195-1207.

Giammarinaro M.S., A. Tertulliani, G. Galli, M. Leta, (2005): Investigation of surface geology and intensity variability in the Palermo, Italy, urban area after the September 6, 2002 earthquake, *Bull. Seism. Soc. Am.*, **95**, no. 6, 2318-2327.

Grünthal, G., (ed.), (1998). European Macroseismic Scale 1998 (EMS-98), European Seismological Commision, subcommission on Engineering Seismology, working Group Macroseismic Scales. Conseil de l'Europe, Cahiers du Centre Européen de Géodynamique et de Séismologie, **15**, Luxembourg, 99 pp.

Guidoboni, E., D. Mariotti, M.S. Giammarinaro, and A. Rovelli A. (2003). Identification of amplified damage zones in Palermo, Sicily (Italy) during the earthquakes of the last three hundred years, *Bull. Seism. Soc. Am.,* **93**, no. 4, 1649-1669.

Haskell, N.A. (1953). The dispersion of surface waves on multilayered media, *Bull. Seism. Soc. Am.*, **43**, no. 1, 17-34.

Koller M.G., Chatelain J.-L., Guillier B., Duval A.M., Atakan K., Lacave C., Bard P.-Y. and the SESAME participants (2004). Practical user guideline and software for the implementation of the H/V ratio technique on ambient vibrations: measuring conditions, processing method and results interpretation. *13th World Conference on Earthquake Engineering* Vancouver, B.C., Canada August 1-6, 2004 Paper No. 3132.

Konno, K., and T. Ohmachi (1998). Ground-motion characteristics estimated from spectral ratio between horizontal and vertical components of microtremor, *Bull. Seism. Soc. Am.*, **88**, no. 1, 228-241.

Lachet, C., D. Hatzfeld, P.-Y. Bard, N. Theodulidis, C. Papaioannou, and A. Savvaidis (1996). Site effects and microzonation in the city of Thessaloniki (Greece). Comparison of different approaches, *Bull. Seism. Soc. Am.* **86**, no. 6, 1692-1703.

Lebrun, B., D. Hatzfeld and P.-Y. Bard (2001). A site effect study in urban area: experimental results in Grenoble (France), *Pure and appl. Geophys.,* **158**, 2543-2557.

Malischewky, P. G., and Scherbaum, F. (2004), Love's formula and H/V ratio (ellipticity) of Rayleigh waves, *Wave Motion*, **40**, 57-67.

Mucciarelli, M. and M.R. Gallipoli (2001), A critical review of 10 years of microtremors HVNSR technique, *Boll. Geof. Teor. Appl.*, **42**(3-4), 255-366.

Nakamura, Y. (1989). A method for dynamic characteristics estimation of subsurface using microtremor on the ground surface, *QR of RTRI,* **30**, 25-33.

Panou, A., N. Theodulidis, P. Hatzidimitriou, A. Savvaidis and C. Papazachos (2005), Reliability of ambient noise horizontal-to-vertical spectral ratio in urban environments: The case of Thessaloniki city (Northern Greece), *Pure and appl. Geophys.*, **162**, no. 5, 891-912.

Rao, C. Radhakrishna (1973), Linear Statistical Inference and Its Applications, 2d ed., John Wiley & Sons, New York.

Satoh, T., H. Kawase and S. Matsushima (2001), Differences between site characteristics obtained from microtremors, S-waves, P-waves, and codas, *Bull. Seism. Soc. Am.*, **91**, no. 2, 313-334.

Seo, K. (1998). Applications of microtremors as a substitute of seismic motion – reviewing the recent microtremors joint research in different sites. In: Irikura, K., Kudo, K., Okada, H., Sasatani, T. (Eds.), *The Effects of Surface Geology on Seismic Motion*, Yokohama, December 1-3, 1998, Balkema, Rotterdam, 577-586.

SESAME Project; see Web site: http://sesame-fp5.obs.ujf-grenoble.fr, 2001.

SESAME Project – Deliverable D01.02 – Final Report of the Instrument Workshop 22-26 October 2001 University of Bergen, Norway – WP02 Controlled Instrumental Specifications, available from the web site: http://sesame-fp5.obs.ujf-grenoble.fr/Delivrables/D01-02_Texte.pdf, 2002.

SESAME Project – Deliverable D08.02 – Final report on Measurement Guidelines – WP02 H/V technique: Experimental conditions, available from the web site: http://sesame-fp5.obs.ujf-grenoble.fr/Delivrables/D08-02_Texte.pdf, 2003.

SESAME Project – Deliverable D09.03 – Report on the Multiplatform H/V Processing Software J-Sesame - WP03 H/V Technique: Data Processing, available from the web site: http://sesame-fp5.obs.ujf-grenoble.fr/Delivrables/D09-03_Texte.pdf, 2003.

SESAME Project – Deliverable D16.04 – Report of the WP04 H/V Technique: Empirical evaluation, available from the web site: http://sesame-fp5.obs.ujf-grenoble.fr/Delivrables/D16-04.pdf, 2004.

SESAME Project – Deliverable D23.12 – Guidelines for the Implementation of the H/V Spectral Ratio Technique on Ambient Vibrations Measurements, Processing and Interpretation, available from the web site: http://sesame-fp5.obs.ujf-grenoble.fr/Papers/HV_User_Guidelines.pdf, 2004.

Teves-Costa, P., I.M. Almeida, and P.L. Silva (2001), Microzonation of Lisbon: 1D theoretical approach, *Pure and appl. Geophys.*, **158**, 2579-2596.

Thomson, W. T. (1950). Trasmission of elastic waves through a stratified solid medium, *Jour. Appl. Phys.*, 21-89.

Figure Captions

Fig. 1 - Map of downtown Palermo, surrounded by the ancient wall, showing zones with different geology. Positions of available boreholes are represented, each with a symbol indicating the main finding of the logs. Kemonia and Papireto are the names of two rivers filled in the 17th century. The position of the Oreto river is also shown. Black lines represent five profiles of noise measurements (A-A', B-B', D-D', E-E' in downtown Palermo and C-C' in the Oreto valley). A grid of measurements was also performed in the confluence zone of the Papireto and Kemonia rivers. Black-solid triangles are some of the stations deployed by Di Giulio et al. (2005) that recorded small magnitude earthquakes during the 2002 sequence.

Fig. 2 – Examples of microtremor spectra at six sites. The mean HVNSR is computed as an average over some tens of time windows. In each panel, Fourier amplitude spectra of the three motion components (in arbitrary counts), computed in a 30-sec window, are shown at the top; the horizontal-to-vertical ratios are shown at the bottom, separately for the two horizontal components (EW/V and NS/V). The shaded area represents the average HVNSR +/- 1 standard deviation of the entire microtremor measurement at each site. For the position of the six sites see Figure 3 (site FF75 is within the grid in the confluence zone).

Fig. 3 - HVNSR results in downtown Palermo. Panels show the classification of each site based on the resonance frequency (top) and the corresponding amplitude (bottom) of HVNSRs, overlain on the geological subdivision of the studied area (see Figure 1). Black dashed lines are geological cross sections (a-a', b-b', d-d', e-e') fitting the microtremor profiles (A-A', B-B', D-D', E-E').

Fig. 4 – Comparison between the HVNSR results and the geological sections a-a', b-b', d-d', e-e'. For each noise measurement profile (A-A', B-B', D-D', E-E'), representative HVNSR curves, the distribution of the resonance frequency (horizontal dash lines indicate the separation between classes) and the geological cross-section are shown. Black vertical lines in the geological cross-sections indicate the boreholes.

Fig. 5 – a) 2D model of profile A-A'. Triangles are measurement sites; crosses and circles indicate the depths from boreholes of the man-made infill and alluvial deposits, respectively. Refer to Table 1 for the seismic parameters of soil 1 (Flysh), 2 (calcarenites), 3 (alluvial deposits) and 4 (fills); b) Contour plots of HVNSRs along the profile A-A'; c) Response for delta-like SH-waves from the 2D model of profile A-A'; d) Comparison of 2D (black line) theoretical transfer functions with HVNSRs (average ± 1 standard deviation, gray lines) for sites #3, #6, #16. For sites #3 and #16 the empirical transfer functions obtained from earthquakes by Di Giulio et al. (2005) for stations PAL2 and PAL6 respectively are overlain (black dashed line).

Fig. 6 - Results of the HVNSR analysis in the Oreto River valley. Top panel: black squares represent HVNSR without frequency peaks or with amplitude values less than 2; white squares represent HVNSR with significant frequency peaks (class 1 means 1.2-1.8Hz). Size of squares is proportional to the value of HVNSR peak. Colored dots are the available boreholes in the area, indicating presence (red) or absence (blue) of alluvial deposits. Note the position of the Norman bridge with respect to the current position of the Oreto River. Dashed red line is the trace of the reconstructed geological cross section CC' (in the bottom panel). Bottom panel: the three HVNSR curves (mean and standard deviations for sites #41, #45 and #49) are representative of the three spectral shapes found west, inside and east of the Oreto River valley. For site #45 the 1D theoretical transfer functions is also shown (dashed line). The geological model used to perform the 1D simulation consists of 7 meters of fill and 42 meters of alluvial deposits overlaying the bedrock. Refer to Table 1 for shear wave velocities of the soils.

Fig. 7 - Damage map of the 1726 earthquake (taken from Guidoboni et al., 2003) with overlapped (a) frequency (circles) and (b) amplitude (squared) of HVNSR results as obtained in the sites of microtremor measurement. The damage colour scale is explained in Table 2.

Fig. 8 - Histograms of occurrence of frequency peaks and related amplitudes as a function of EMS damage grade for (a) the 1726 earthquake and (b) the cumulative damage of three earthquakes (Guidoboni et al., 2003), both computed in 100m x 100m cells.

Fig. 9 – (a) Proportion of total variance accounted for by each factor, derived from the corresponding eigenvalue; (b) cumulative variance.

Fig. 10 – Factor loadings of original variables into (a) factor 1 and (b) factor 2. The HVNSR amplitude variables are the mean values computed in the nine frequency intervals from 0.5 to 5Hz. The first two damage variables refer to the 1726 and 1823 earthquakes, the third refers to the cumulative damage value of the 1726, 1823 and 1940 events. The combination of the two panels indicate that (panel a) HVNSR amplitude variables are in direct correlation with the damage grade in the low-medium frequency band (0.5-3.0 Hz), and (panel b) HVNSR amplitude variables in the high frequency band (3-5 Hz) are not correlated with damage grades.

Fig. 11 – Spatial distribution of factor 1 values. The pattern reflects the position of the two filled river-beds (compare Figure 1).

Fig. 12 – Results of the best canonical correlation between damage and HVNSR amplitude variables. (a) Values of canonical correlation vector $[A]$, representing the weights of the damage variables; (b) values of vector $[B]$, representing the weights of the HVNSR variables.

Fig. 13 – (a) Correlation between the canonical variable $[X_{can}]$ representing a linear combination of original HVNSR variables and the canonical variable $[Y_{can}]$ representing a linear combination of the EMS damage grades of the earthquakes studied. Linear fit equation: $y_{can} = (0.72 \pm 0.08)x_{can} + (1.62 \pm 0.14)$; goodness of fit $R^2 = 0.51$; F test on regression: $F = 80.53$ significant at the $\alpha =$ 0.01 level of significance (degrees of freedom 1 and 76). (b) Distribution of values of $[Y_{can}]$; the bimodal pattern permits the definition of a threshold (vertical straight-line) that separates negligible from important damage.

Fig. 14 - Spatial distribution of canonical variable $[Y_{can}]$. White and black dots represent values respectively below and above the damage threshold (2.7). As in Figure 11, the canonical analysis confirms the high correlation among local geology, observed damage and the HVNSR results.

Table 1. Velocity model used for the simulations.

	soil type	Vs (m/s)	Rho (g/cm3)	Q
1	Flysh (bedrock)	1200	2.2	1000
2	Calcarenites	400	2.1	33
3	Alluvial deposits	200-250	1.9	10-20
4	Fills	100	1.8	5-10
5	Quarry fills	200	1.9	20

Table 2. Translation of the damage colour scale of Guidoboni et al. (2003) into the EMS 1998 scale.

Guidoboni et al. 2003	**EMS: description of damage to masonry buildings**	**Colour scale**	**EMS classification**
No damage	–	white	
Slight damage cracks to the plastering, collapse of ornamental or protruding elements	**Negligible to slight damage (no structural damage, slight non-structural damage)** Hair-line cracks in very few walls. Fall of small pieces of plaster only. Fall of loose stones from upper parts of buildings in very few cases.	yellow	**Grade 1**
Moderate damage fissures to inside walls, collapse of vaults or ceilings	**Moderate damage (slight structural damage, moderate non-structural damage)** Cracks in many walls. Fall of fairly large pieces of plaster. Partial collapse of chimneys.	orange	**Grade 2**
Serious damage total collapses, deep fissures, disconnections, leaning walls	**Substantial to heavy damage (moderate structural damage, heavy non-structural damage)** Large and extensive cracks in most walls. Roof tiles detach. Chimneys fracture at the roof line; failure of individual non-structural elements (partitions, gable walls)	red	**Grade 3**
Very serious damage total collapse of the buildings or most of it	**Very heavy damage (heavy structural damage, very heavy non-structural damage)** Serious failure of walls; partial structural failure of roofs and floors	purple	**Grade 4**:
–	**Destruction (very heavy structural damage)** Total or near total collapse	–	**Grade 5**

Table 3. Significance test to assess the validity of each canonical correlation

Canonical variable	Canonical correlation	Raos F	Numerator degrees of freedom	Denominator degrees of freedom	Larger F probability
1	0.7173	2.632	27	193.4	0.0001
2	0.3298	0.842	16	134.0	0.6365
3	0.2713	0.772	7	68.0	0.6130

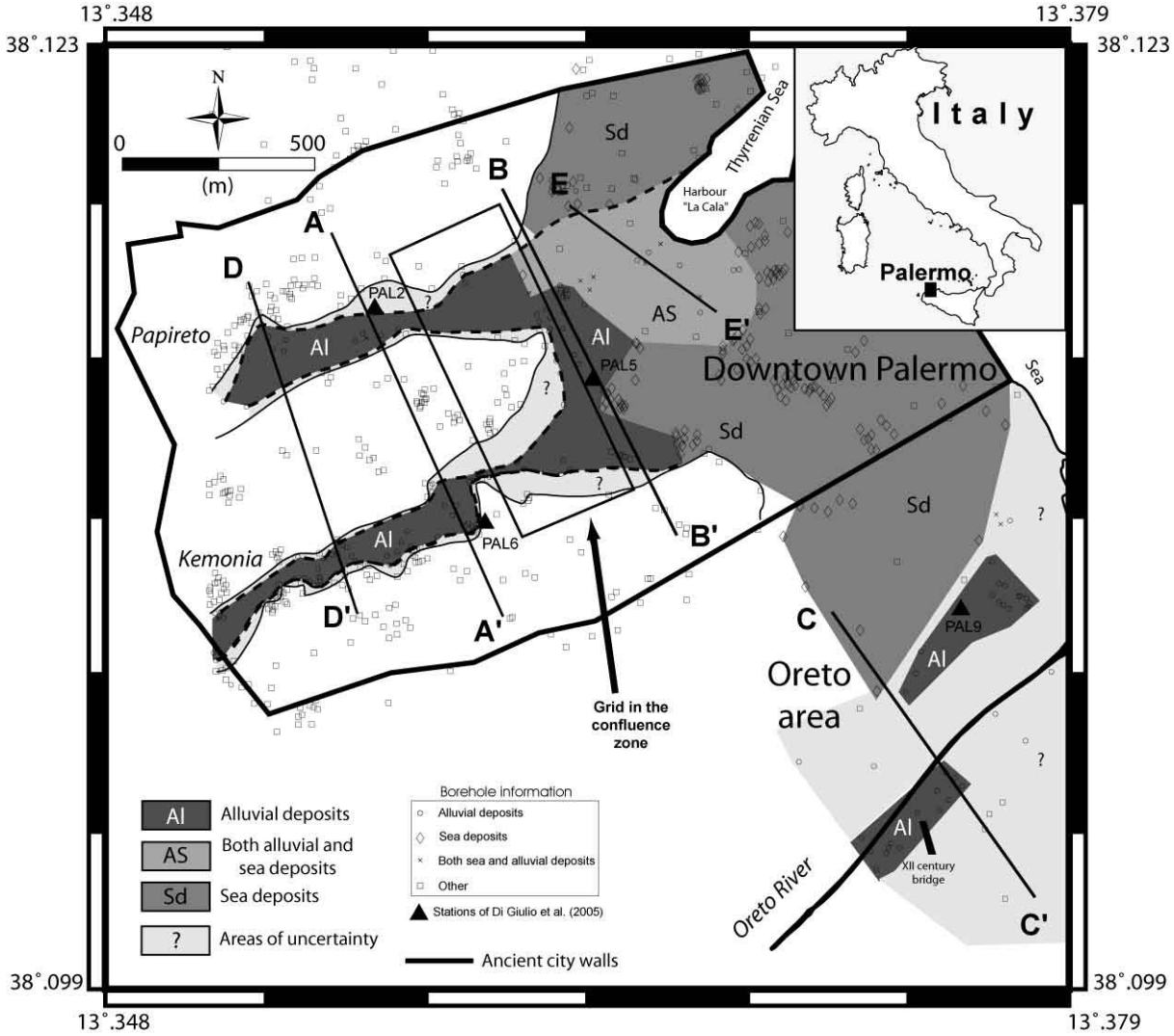
13°.348
13°.379
38°.123
38°.123
38°.099
38°.099
13°.348
13°.379
N
0
500
(m)
Sd
Thyrrenian Sea
Harbour "La Cala"
B
E
A
D
PAL2
Papireto
Al
AS
E'
Al
PAL5
Downtown Palermo
Sea
Sd
Sd
Sd
B'
Kemonia
Al
PAL6
D'
A'
C
PAL9
Al
Oreto area
Grid in the confluence zone
Al
XII century bridge
Oreto River
C'
Italy
Palermo
Borehole information
Alluvial deposits
Sea deposits
Both sea and alluvial deposits
Other
Stations of Di Giulio et al. (2005)
Al
Alluvial deposits
AS
Both alluvial and sea deposits
Sd
Sea deposits
?
Areas of uncertainty
Ancient city walls

Figure 1

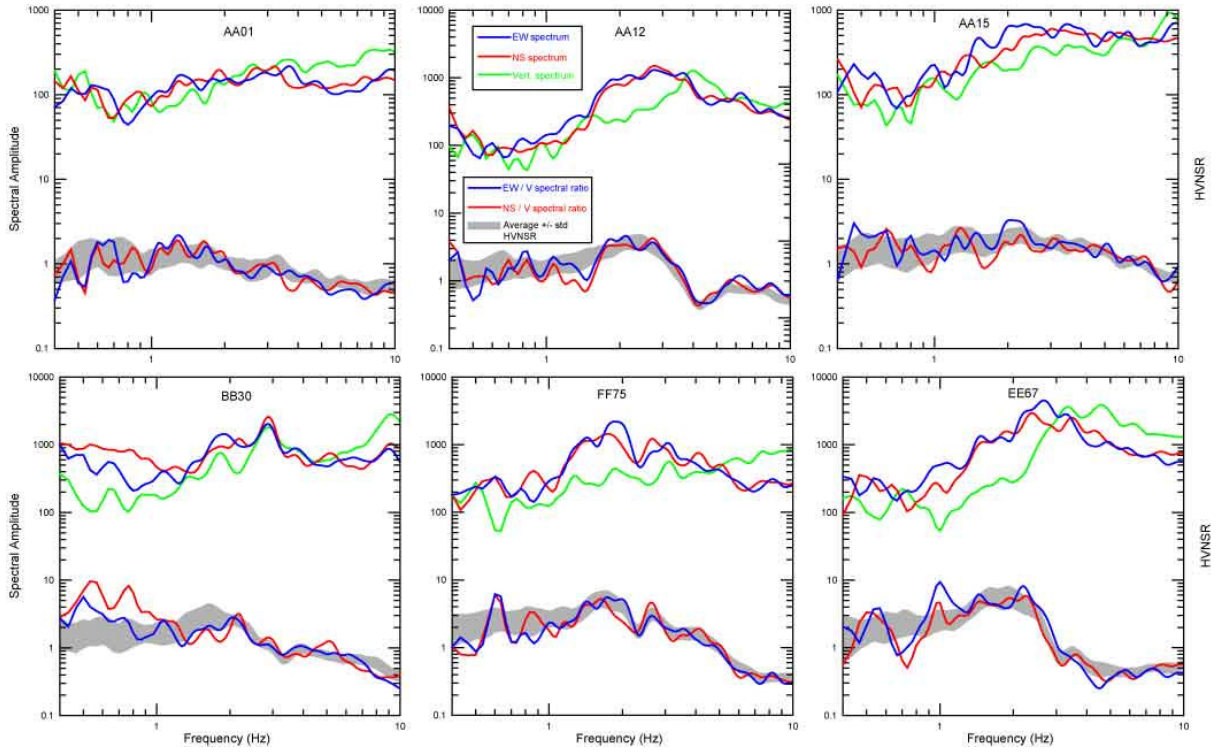
AA01
AA12
AA15
BB30
FF75
EE67
EW spectrum
NS spectrum
Vert. spectrum
EW / V spectral ratio
NS / V spectral ratio
Average +/- std
HVNSR
Spectral Amplitude
HVNSR
Frequency (Hz)

Figure 2

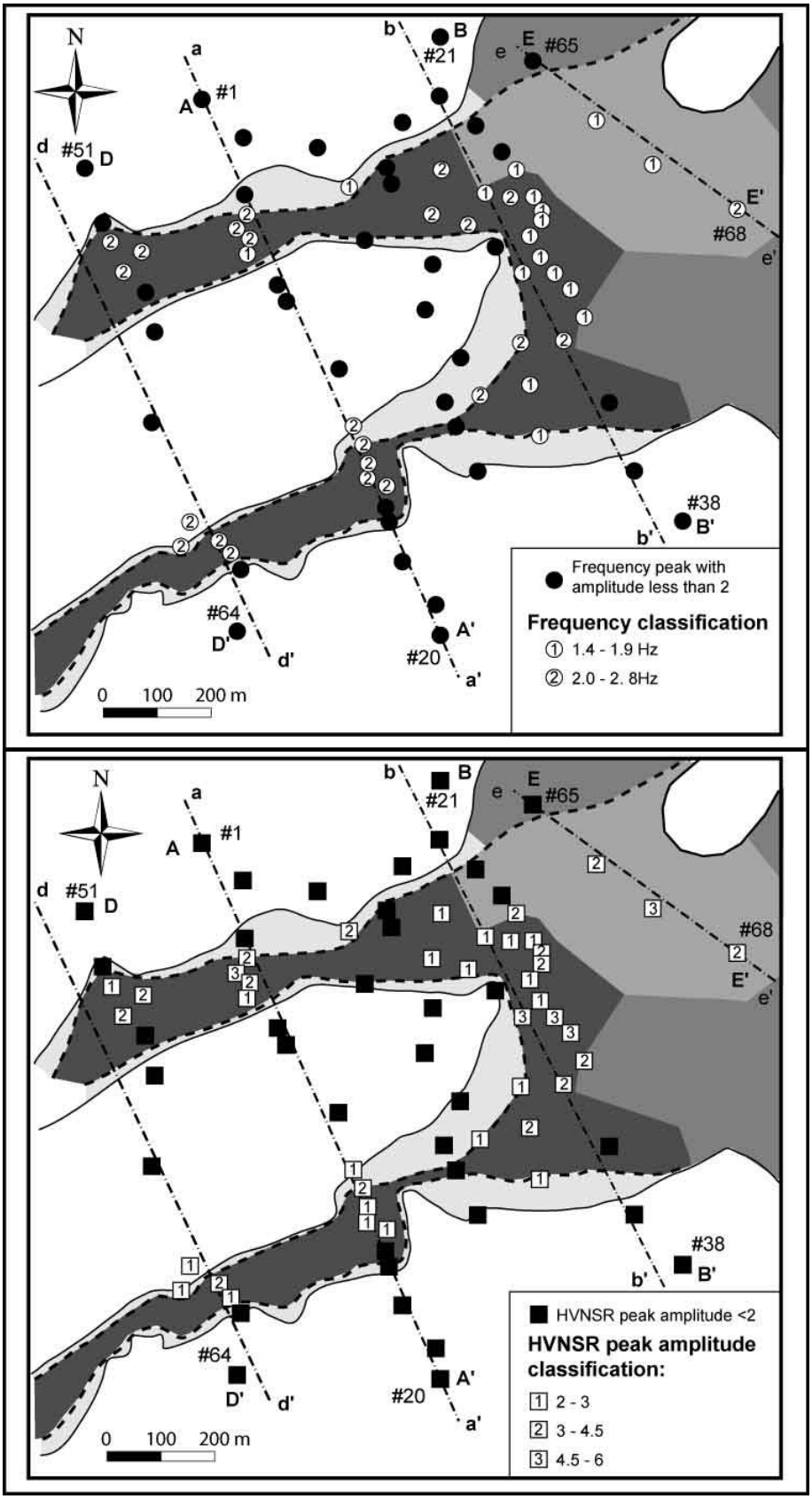
N
a
A
#1
b
B
#21
e
E
#65
d
#51
D
E'
#68
e'
#38
B'
b'
Frequency peak with amplitude less than 2
Frequency classification
① 1.4 - 1.9 Hz
② 2.0 - 2. 8Hz
#64
D'
d'
A'
#20
a'
0 100 200 m
HVNSR peak amplitude <2
HVNSR peak amplitude classification:
1 2 - 3
2 3 - 4.5
3 4.5 - 6

Figure 3

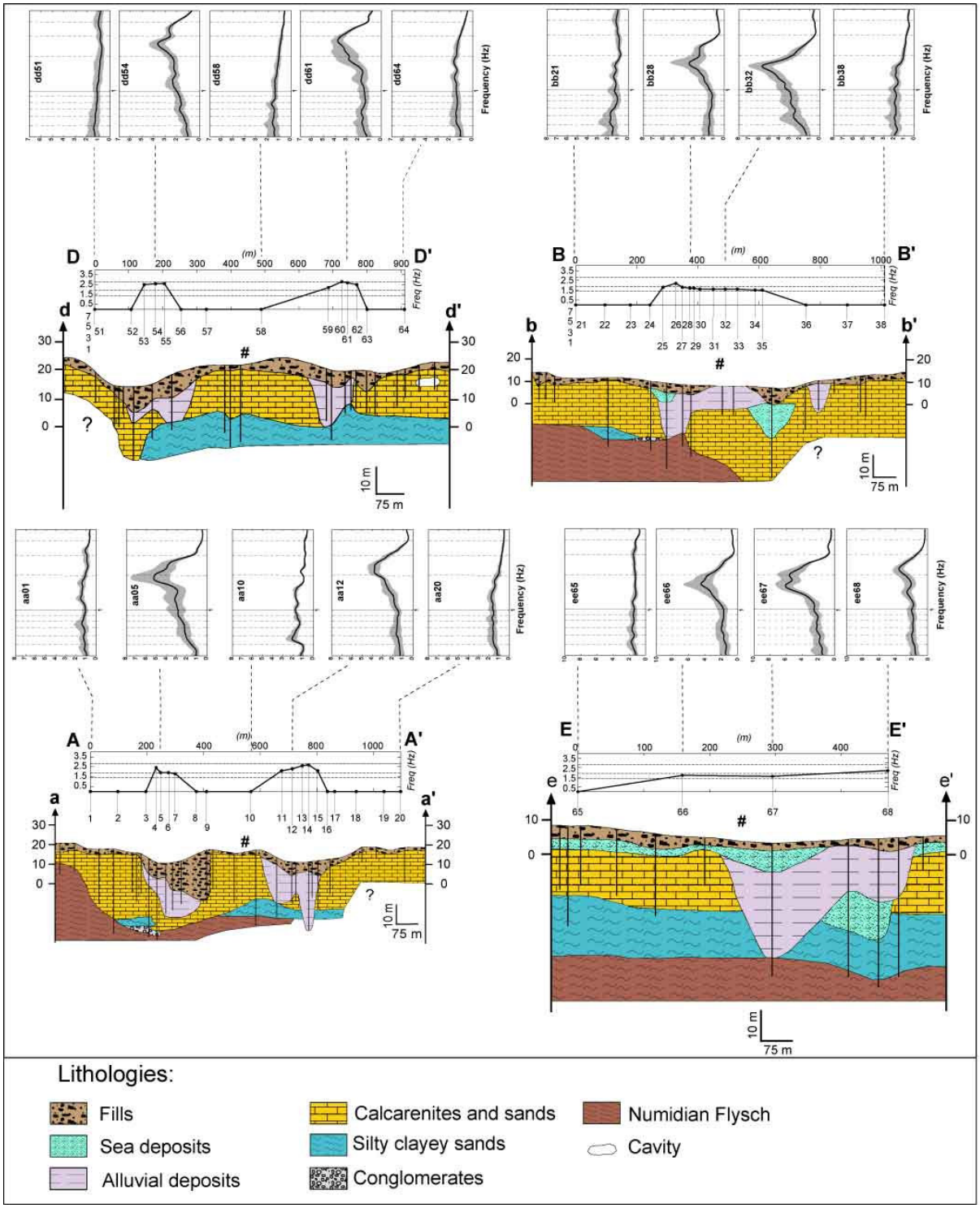
dd51
dd54
dd58
dd61
dd64
Frequency (Hz)
bb21
bb28
bb32
bb38
Frequency (Hz)
D
D'
(m)
Freq (Hz)
d
d'
B
B'
b
b'
10 m
75 m
aa01
aa05
aa10
aa12
aa20
Frequency (Hz)
ee65
ee66
ee67
ee68
Frequency (Hz)
A
A'
a
a'
E
E'
e
e'
Lithologies:
Fills
Sea deposits
Alluvial deposits
Calcarenites and sands
Silty clayey sands
Conglomerates
Numidian Flysch
Cavity

Figure 4

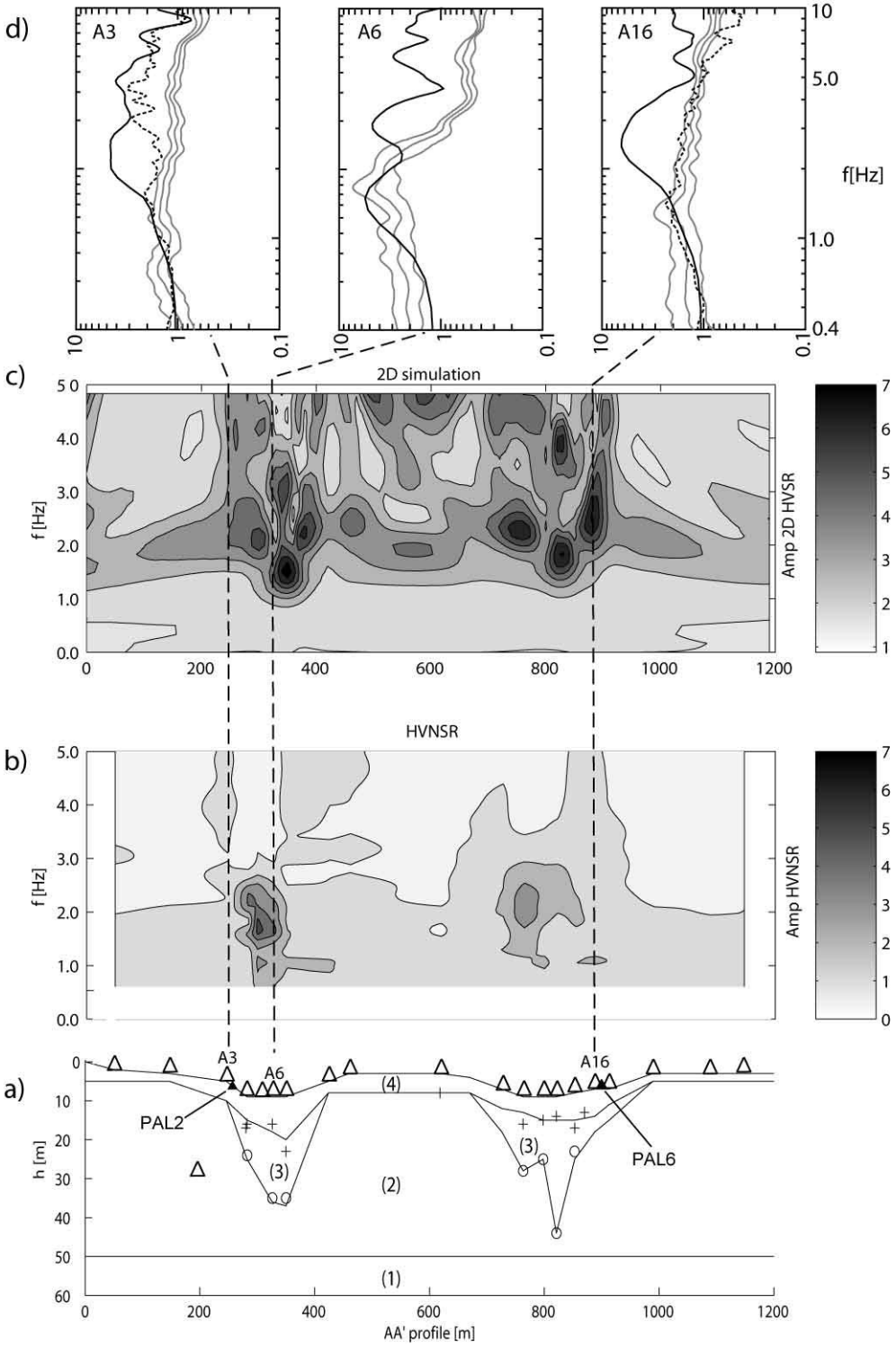
d)
A3
A6
A16
10
5.0
1.0
0.4
f[Hz]
c)
2D simulation
f [Hz]
Amp 2D HVSR
b)
HVNSR
Amp HVNSR
a)
PAL2
PAL6
(1)
(2)
(3)
(4)
h [m]
AA' profile [m]

Figure 5

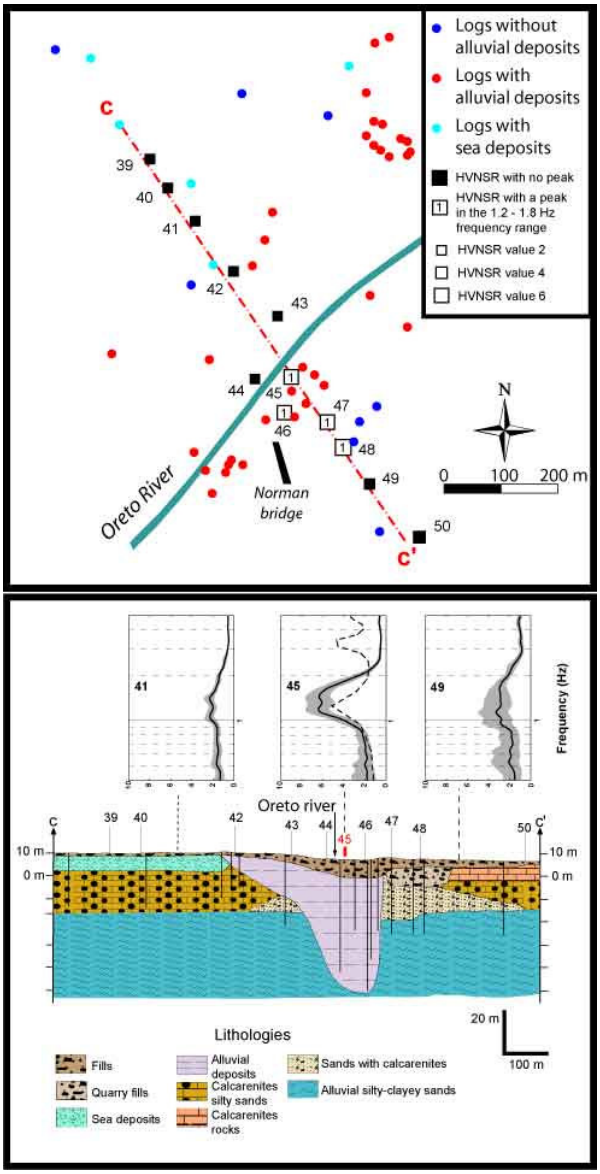
Logs without alluvial deposits
Logs with alluvial deposits
Logs with sea deposits
HVNSR with no peak
HVNSR with a peak in the 1.2 - 1.8 Hz frequency range
HVNSR value 2
HVNSR value 4
HVNSR value 6
C
C'
39
40
41
42
43
44
45
46
47
48
49
50
Oreto River
Norman bridge
N
0 100 200 m
41
45
49
Frequency (Hz)
Oreto river
10 m
0 m
20 m
100 m
Lithologies
Fills
Quarry fills
Sea deposits
Alluvial deposits
Calcarenites silty sands
Calcarenites rocks
Sands with calcarenites
Alluvial silty-clayey sands

Figure 6

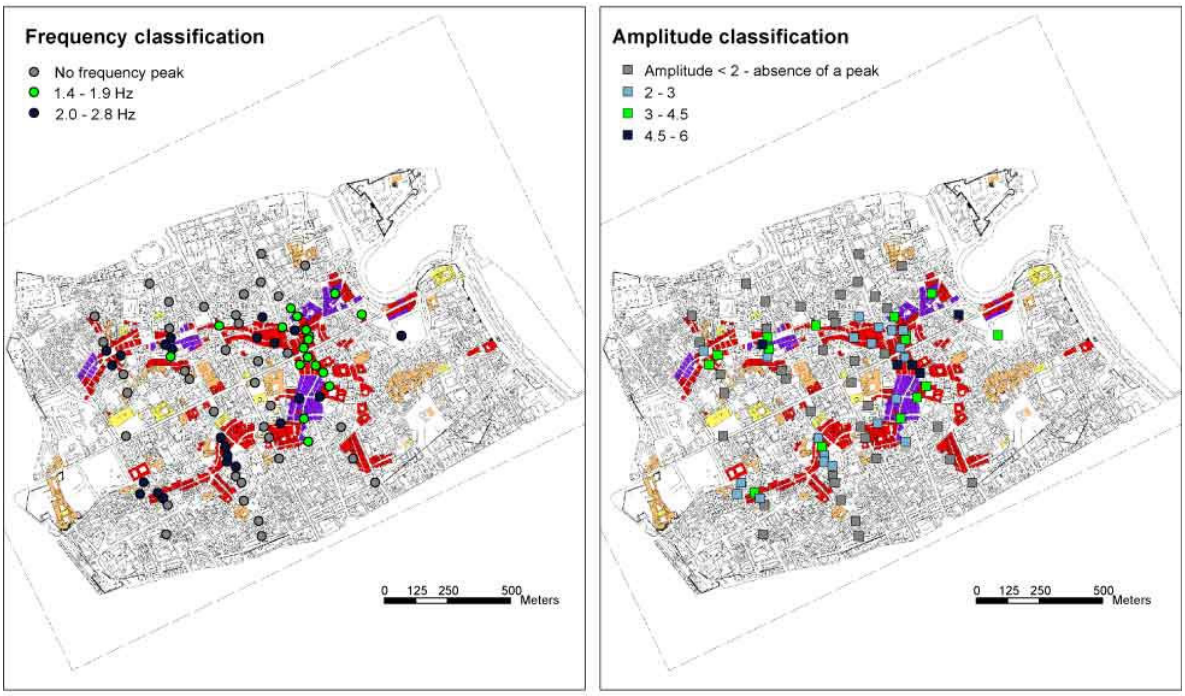
Frequency classification
No frequency peak
1.4 - 1.9 Hz
2.0 - 2.8 Hz
0 125 250 500
Meters
Amplitude classification
Amplitude < 2 - absence of a peak
2 - 3
3 - 4.5
4.5 - 6
0 125 250 500
Meters

Figure 7

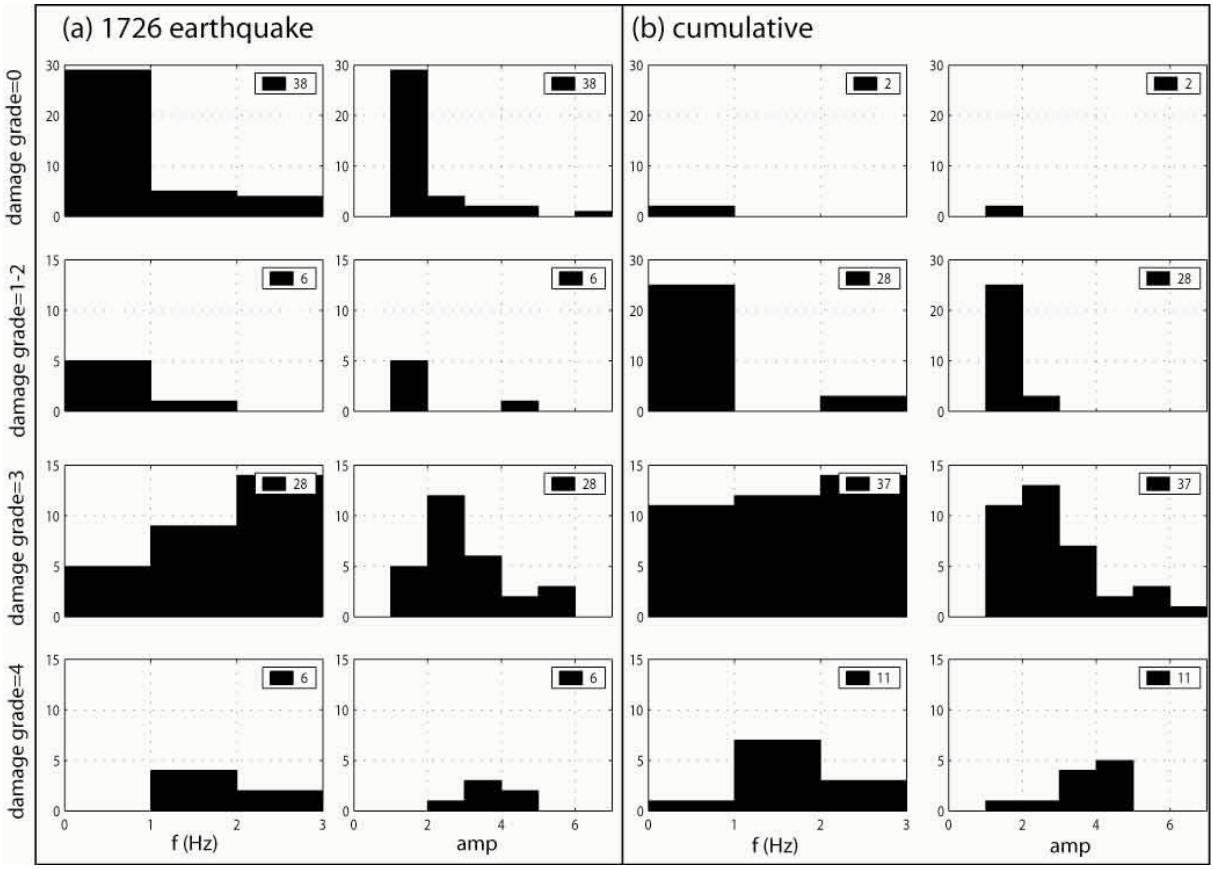
(a) 1726 earthquake
(b) cumulative
damage grade=0
damage grade=1-2
damage grade=3
damage grade=4
38
38
2
2
6
6
28
28
28
28
37
37
6
6
11
11
f (Hz)
amp
f (Hz)
amp

Figure 8

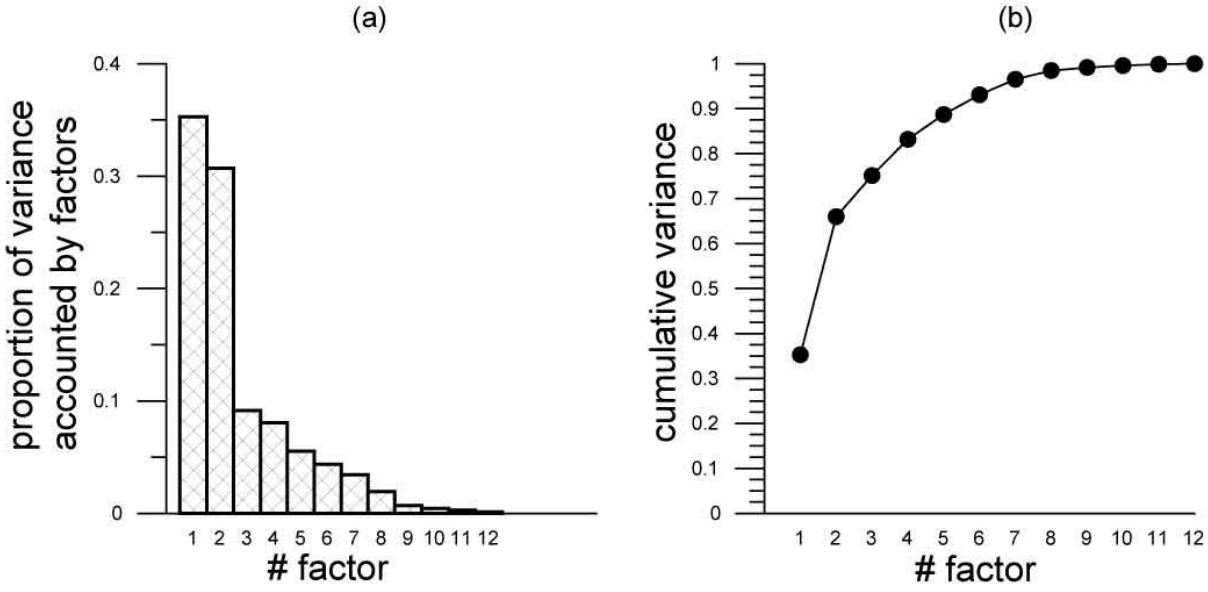
(a)
proportion of variance accounted by factors
0.4
0.3
0.2
0.1
0
1 2 3 4 5 6 7 8 9 10 11 12
factor
(b)
cumulative variance
1
0.9
0.8
0.7
0.6
0.5
0.4
0.3
0.2
0.1
0
1 2 3 4 5 6 7 8 9 10 11 12
factor

Figure 9

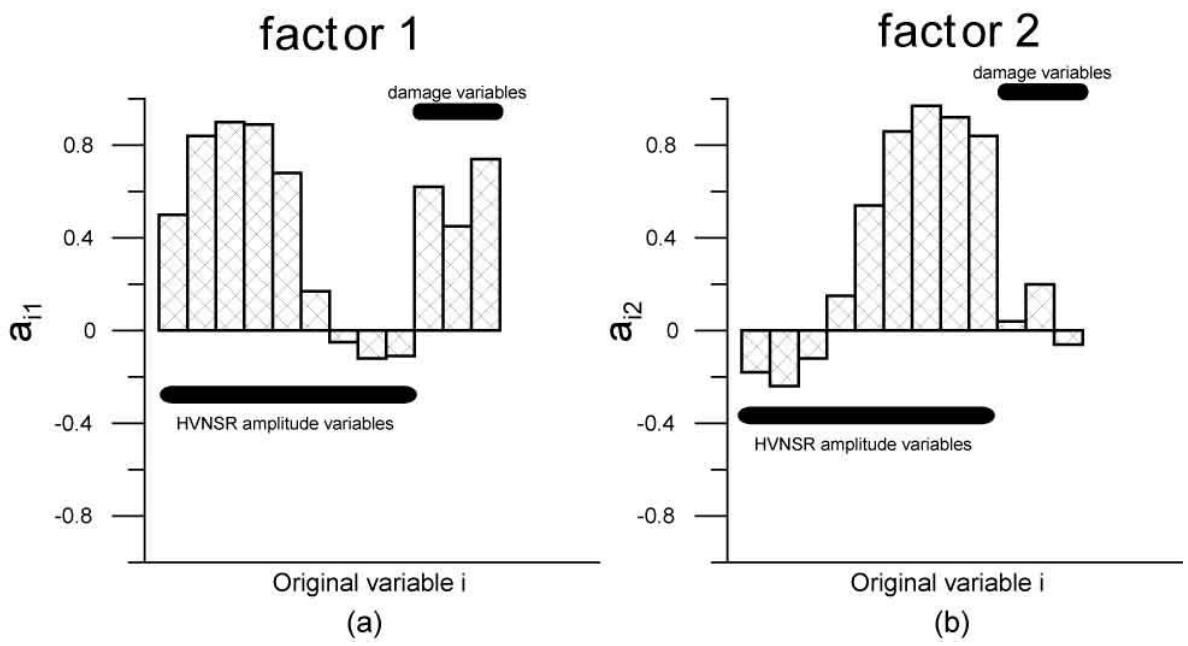
factor 1
damage variables
0.8
0.4
0
-0.4
-0.8
a_{i1}
HVNSR amplitude variables
Original variable i
(a)
factor 2
damage variables
0.8
0.4
0
-0.4
-0.8
a_{i2}
HVNSR amplitude variables
Original variable i
(b)

Figure 10

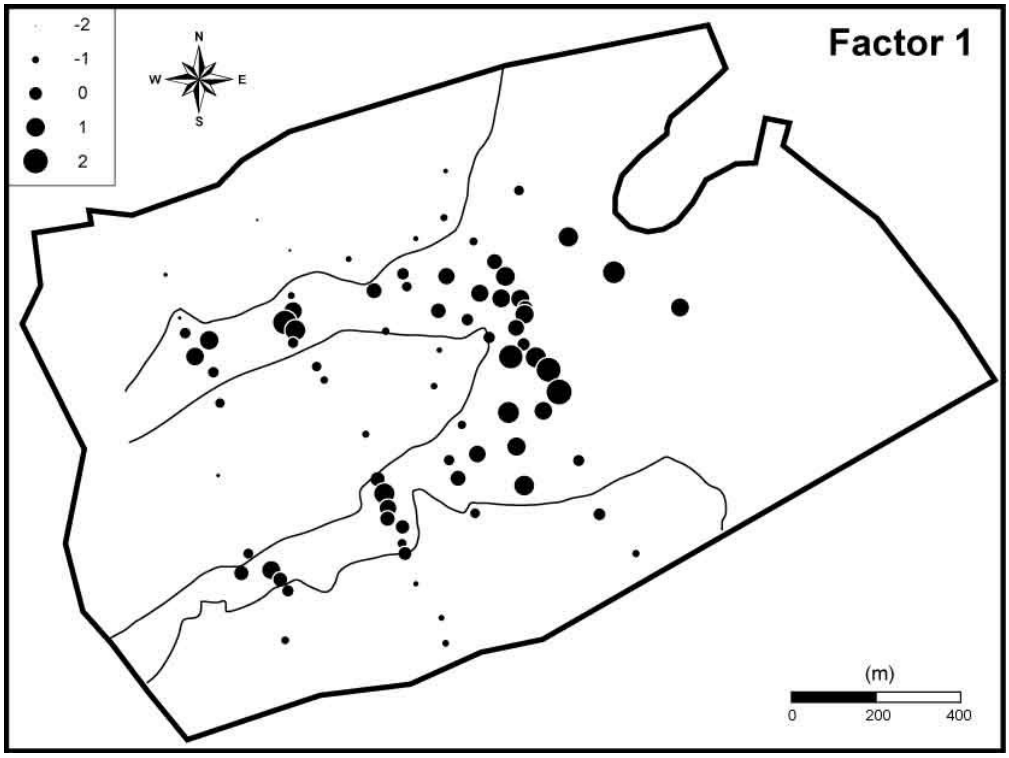

Figure 11

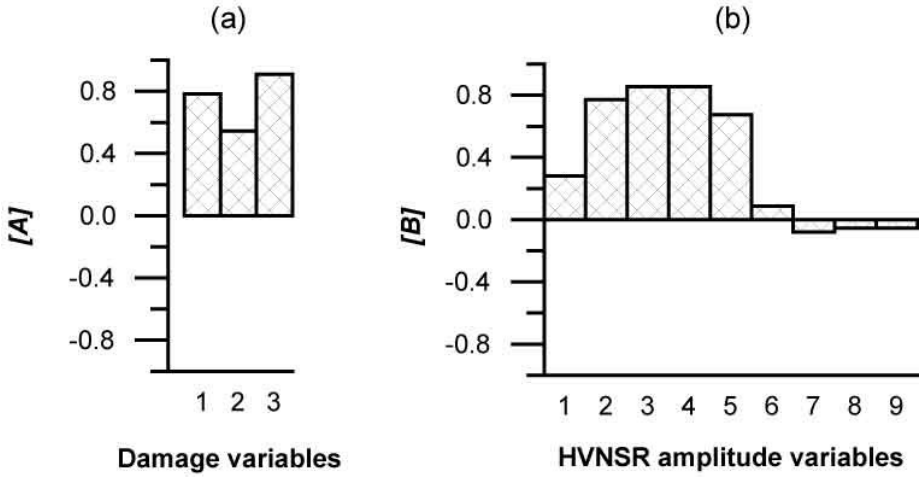
(a)
(b)
0.8
0.4
0.0
-0.4
-0.8
[A]
[B]
1 2 3
1 2 3 4 5 6 7 8 9
Damage variables
HVNSR amplitude variables

Figure 12

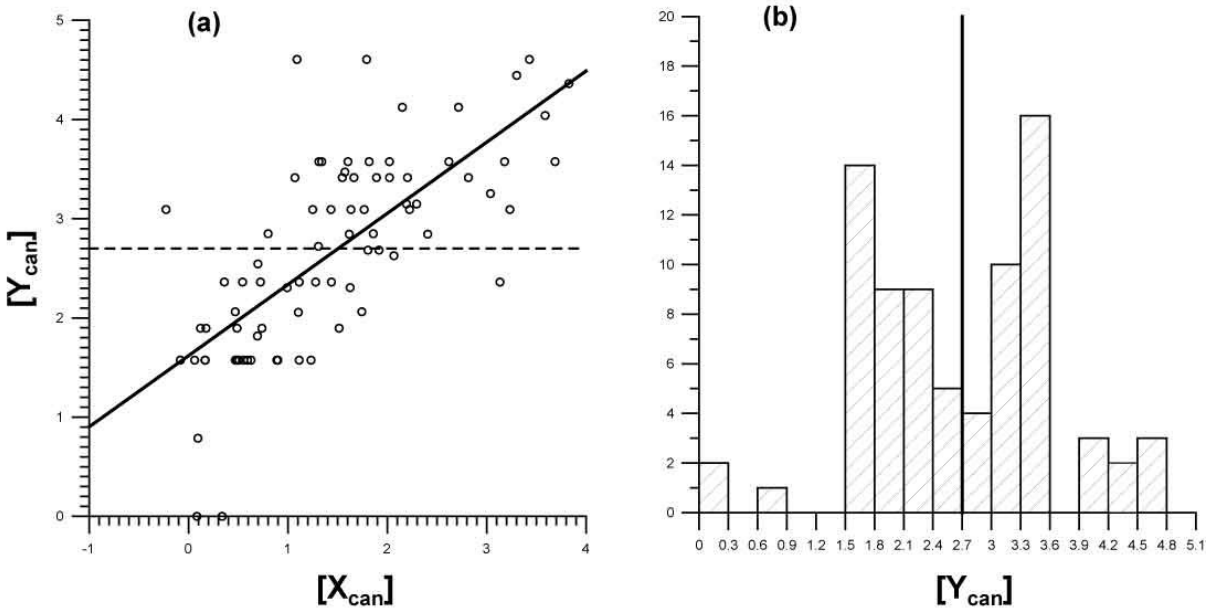

Figure 13

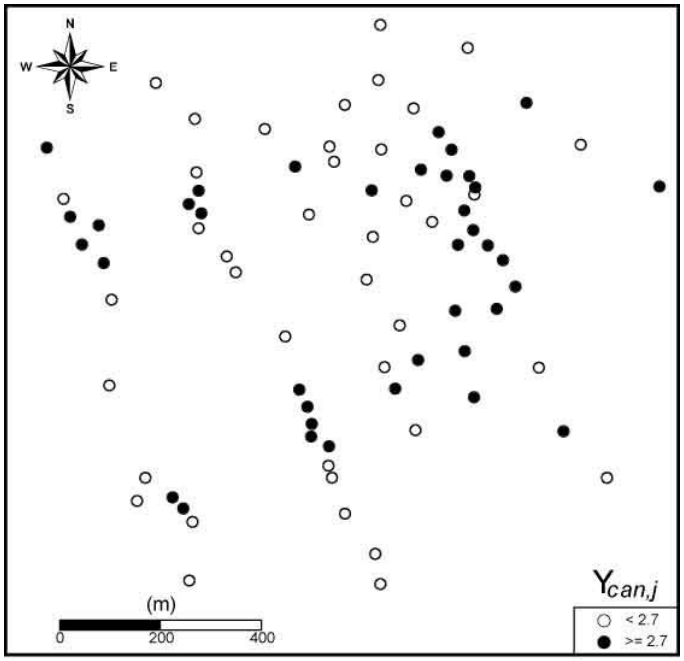

Figure 14